Applied Radiation and Isotopes 89 (2014) 102–108

Contents lists available at ScienceDirect

Applied Radiation and Isotopes

journal homepage: www.elsevier.com/locate/apradiso

Development and calibration of a real-time airborne radioactivity monitor using direct gamma-ray spectrometry with two scintillation detectors

R. Casanovas [a,*], J.J. Morant [b], M. Salvadó [a]

[a] Unitat de Física Mèdica, Facultat de Medicina i Ciències de la Salut, Universitat Rovira i Virgili, ES-43201 Reus, Tarragona, Spain
[b] Servei de Protecció Radiològica, Servei de Recursos Científics i Tècnics, Universitat Rovira i Virgili, ES-43007 Tarragona, Spain

HIGHLIGHTS

- A real-time airborne radioactivity monitor was developed.
- The monitor is formed using two scintillation detectors for gamma-ray spectrometry.
- The detectors are shielded with Pb. One detector is pointing up and the other down.
- The monitors were calibrated using experimental data and Monte Carlo simulations.
- The efficiency calculations and MDAC values are given.

ARTICLE INFO

Article history:
Received 24 September 2013
Received in revised form
8 January 2014
Accepted 28 January 2014
Available online 12 February 2014

Keywords:
Scintillation gamma-ray spectrometry
NaI(Tl)
$LaBr_3$(Ce)
Monte Carlo simulation
Efficiency calculation

ABSTRACT

The implementation of in-situ gamma-ray spectrometry in an automatic real-time environmental radiation surveillance network can help to identify and characterize abnormal radioactivity increases quickly. For this reason, a Real-time Airborne Radioactivity Monitor using direct gamma-ray spectrometry with two scintillation detectors (RARM-D2) was developed. The two scintillation detectors in the RARM-D2 are strategically shielded with Pb to permit the separate measurement of the airborne isotopes with respect to the deposited isotopes.In this paper, we describe the main aspects of the development and calibration of the RARM-D2 when using NaI(Tl) or $LaBr_3$(Ce) detectors. The calibration of the monitor was performed experimentally with the exception of the efficiency curve, which was set using Monte Carlo (MC) simulations with the EGS5 code system. Prior to setting the efficiency curve, the effect of the radioactive source term size on the efficiency calculations was studied for the gamma-rays from ^{137}Cs. Finally, to study the measurement capabilities of the RARM-D2, the minimum detectable activity concentrations for ^{131}I and ^{137}Cs were calculated for typical spectra at different integration times.

1. Introduction

The Euratom Treaty requires each Member State to establish the necessary facilities to carry out real-time monitoring of the level of radioactivity in the air, water and soil and to ensure compliance with the basic standards (2000/473/Euratom, 2000). Following these requirements, there is an automatic real-time surveillance network in Catalonia (ES-E, Spain-East) that is essentially composed of two types of monitors (Casanovas et al., 2011): aerosol and Geiger monitors. The aerosol monitors provide artificial alpha and beta, radon and gamma (due mainly to the iodine isotopes) activity concentrations. The Geiger monitors provide the ambient dose equivalent rate.

In a previous study (Casanovas et al., 2011), it was identified that the use of in-situ real-time gamma-ray spectrometry would help to identify and characterize abnormal radioactivity increases quickly. In this sense, the isotope identification can distinguish between artificial and natural radioactivity increments, and the quantification can establish alert levels based on the limits provided by legislation.

Thus, three different types of radiation monitors using either NaI(Tl) or $LaBr_3$(Ce) scintillation detectors have been developed recently and implemented into the Catalan surveillance network: a water monitor (Casanovas et al., 2013), an aerosol monitor using a particulate filter (Casanovas et al., 2012c, 2014) and the monitor presented in this study.

Environmental monitoring with real-time gamma-ray spectrometry using scintillation detectors has become fairly common,

* Corresponding author. Tel.: +34 977759382.
E-mail address: ramon.casanovas@urv.cat (R. Casanovas).

http://dx.doi.org/10.1016/j.apradiso.2014.01.026
0969-8043

especially when the measurements are performed directly in the environment (i.e., without needing to concentrate the isotopes in a fiber or charcoal filter). For this purpose, either NaI(Tl) (Aage et al., 2003; Zhang et al., 2013) or $LaBr_3$(Ce) detectors (Toivonen et al., 2008; Mattila et al., 2010) have been used.

However, when measuring directly in the environment, the characterization of the radiation source term in a nuclear release is a demanding task. In particular, it is difficult to know if the contributions to the measured spectra are from a radioactive cloud or from a deposition on the ground.

For this reason, a Real-time Airborne Radioactivity Monitor using Direct gamma-ray spectrometry with two scintillation detectors (RARM-D2) was developed. The RARM-D2 enables the discrimination between the isotopes contained in a radioactive cloud from those deposited or emerging from the ground, which enables a good primary characterization of the radioactivity source term in a nuclear release.

In this work, we describe the main aspects of the development and calibration of the RARM-D2, either using NaI(Tl) or $LaBr_3$(Ce) detectors, with particular emphasis being placed on the efficiency calibration. In addition, several typical spectra are shown, and the measurement capabilities of this monitor were studied for ^{131}I and ^{137}Cs with different integration times and for both detector types.

2. Materials and methods

2.1. Description of the RARM-D2

A general scheme of the developed monitor (Casanovas et al., 2012b) is shown in Fig. 1. The RARM-D2 is formed using two scintillation detectors, one pointing up (1) and the other pointing down (2), which are shielded with Pb (3). This geometrical disposition together with the shielding permits the discrimination between the isotopes contained in a radioactive cloud from those deposited or emerging from the ground, which can be of interest after a nuclear accident to characterize the radiation source term.

The detectors used in this study were two $2'' \times 2''$ NaI(Tl) and two $2'' \times 2''$ $LaBr_3$(Ce) scintillation detectors, which made it possible to have one of each pointing up and down, respectively. The NaI(Tl) detectors were Model 905-3 from ORTEC® and the $LaBr_3$(Ce) detectors were BrilLanCe™380 from Saint-Gobain Crystals. All detectors were connected to a multichannel pulse-height analyzer of 2000 channels. The Pb shielding was specifically designed for this monitor and was manufactured by TECNIBUSA Protección Radiológica S.L.

The system integrates a meteorological station (Davis Vantage Pro2 Weather Station, Davis Instruments Corp., California, U.S.A.) that provides the following data: wind speed and direction, temperature, humidity, barometric pressure, rainfall and solar radiation. The integration of a meteorological station can provide valuable information for studying the evolution of the radiation source term, especially in cases of nuclear accidents.

The system is controlled using a specially designed software in the Delphi programming language. The obtained data are transmitted to a main server via an ADSL connection (using the SSL/TLS protocol), the system is remotely controlled using the TCP/IP protocol. However, other redundant means of communication are possible (GSM, radiofrequency, satellite, etc.). From the main server, it is also possible to activate alternative measurement systems (e.g., high flow filters for laboratory analysis) and to send automatic messages (SMS or emails) to a predefined contact list in response to either radiological criteria or different sensor signals.

2.2. Calibration of the RARM-D2

The calibration methodology for NaI(Tl) and $LaBr_3$(Ce) detectors has been described in detail in a previous paper (Casanovas et al., 2012a) and adapted specifically for this monitor. This methodology encompasses energy, resolution and efficiency calibrations.

2.2.1. Energy and resolution calibrations

The energy and resolution calibrations were established using five radioactive point sources (^{241}Am, ^{133}Ba, ^{137}Cs, ^{60}Co and ^{152}Eu) and complemented with some emissions from natural background isotopes (such as ^{214}Pb, ^{214}Bi, ^{40}K or ^{208}Tl). The detectors were adjusted to cover the energy range from 0 to 3000 keV. The stability of the energy calibration in the systems without automatic gain control was controlled by means of software using the method described in (Casanovas et al., 2012d).

2.2.2. Efficiency calibrations

The efficiency calibration establishes the relationship (for each energy of the gamma-rays) between the number of counts under a peak and the activity (or activity concentration) of a radioactive source. In the RARM-D2, we are interested in measuring volumetric activity (Bq m^{-3}) with the detector pointing up and superficial activity (Bq m^{-2}) with the detector pointing down.

To obtain a complete efficiency curve for each detector and geometrical disposition, efficiency calculations were performed

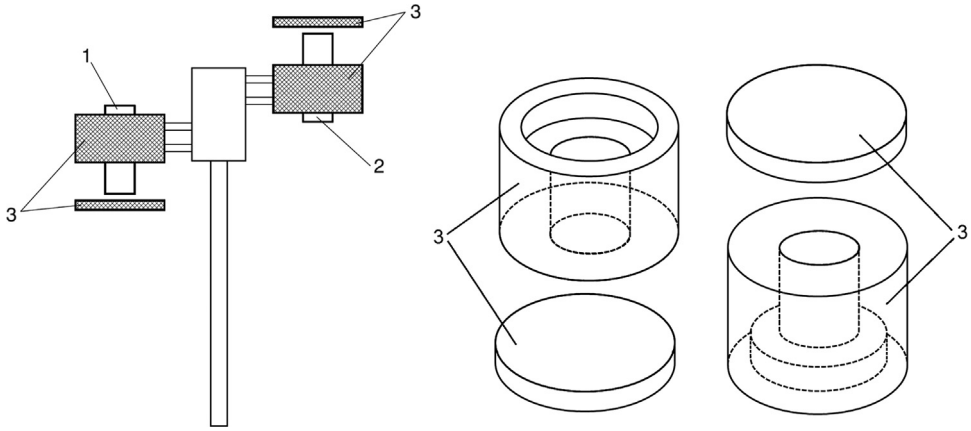

Fig. 1. General scheme of the RARM-D2 (left) and detailed scheme of the Pb shielding (right). The main elements are: detector pointing up (1), detector pointing down (2) and Pb shielding (3).

using MC simulations. The MC simulations were performed with a previously validated EGS5 user code (Casanovas et al., 2012a). This user code contains all of the information about the radiation source (type of particles, energy of the particles, geometrical distribution of the source, etc.) and the involved detection system (type of detector, Pb shielding, etc.).

The simulations were carried out on the CESCA cluster in a Bull NovaScale machine comprised of 224 Xeon E5472 cores and 112 Xeon X5550 cores, 1.6 TB of main memory and 52.6 TB of disk memory. The simulations were performed separately but simultaneously, each using 1 processor and 4 GB of memory.

Thus, a model of the RARM-D2 (see Fig. 2) was implemented for the MC simulations based on the real dimensions and materials, which were taken from the manufacturer technical specifications. Briefly, the geometry was modeled with the corresponding scintillation crystal, either NaI(Tl) or $LaBr_3$(Ce), with a case of 0.5 mm of Al. The space between the case and the crystal was filled with air. A glass light guide after the crystal was also considered, and the photomultiplier tube was modeled as an air-filled cylinder of Al. The tube base was modeled with a mixture of Al and Cu. The material information (density and composition) was taken from the literature (Berger et al., 2005), and the cut-off energy for the photons and the electrons was set at 10 keV.

For the efficiency calculations, each point of each efficiency curve was calculated separately by considering a monoenergetic radiation source (in the range of 20 to 3000 keV). Because the distribution of the radiation source term is not known a priori, a semi-infinite homogeneous activity concentration was assumed. However, the developed simulation user code is ready to accept any distribution of the source term, which can be of interest to provide retrospectively improved activity concentration calculations when more information on the source term evolution becomes available.

Fig. 3 shows the different geometries considered in the MC simulations for both orientations (up and down) of both the NaI (Tl) and $LaBr_3$(Ce) detectors. The radiation source term for the up-detectors is a cylinder of radius R and height $H=2R$ whereas the source term for the down-detectors is a disk of radius R. To set the computational semi-infinite dimensions, the variation of the efficiency values with R was studied for a monoenergetic homogeneous source of 662 keV, which corresponds to the main ^{137}Cs gamma-ray emission. Regarding the obtained results, the final efficiency curves for the RARM-D2 were calculated using $2R=500$ m.

In the MC simulations, the efficiency was calculated as:

$$\varepsilon = \frac{N_{counts}}{N_{hist}} \tag{1}$$

where N_{counts} is the number of net counts under the full energy peak and N_{hist} is the number of simulated histories (i.e., the number of primary source-particles simulated and all of the secondary particles produced by it), which was set at 10^8.

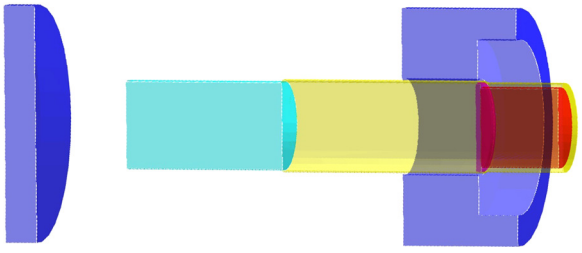

Fig. 2. Geometric model of the RARM-D2 (to scale) used in the MC simulations.

The volumetric efficiencies ε_V for the up-detectors were then calculated as:

$$\varepsilon_V \equiv \varepsilon \times V \tag{2}$$

where ε is the efficiency calculated with Eq. (1) and V the volume of the source term.

In a similar way, the superficial efficiencies ε_S for the down-detectors were calculated as:

$$\varepsilon_S \equiv \varepsilon \times S \tag{3}$$

where ε is the efficiency calculated with Eq. (1) and S the surface of the source term.

Finally, the efficiency calculations were fitted to the following function:

$$\log\ \varepsilon_X = \sum_{n=0}^{6} a_n (\log\ E)^n \tag{4}$$

where ε_X is either the volumetric efficiency ε_V or the superficial efficiency ε_S at the gamma-ray energy E and a_n represents the fitting coefficients.

2.3. Minimum detectable activity concentration (MDAC)

The detection capabilities of a system are usually evaluated with the detection limit L_D or the minimum number of counts under a peak that one can be confident of detecting with a certain probability. Thus, the Minimum Detectable Activity Concentration (MDAC) is the activity concentration equivalent to the detection limit L_D.

After the efficiency calibration, the activity concentration a_X can be calculated as:

$$a_X = \frac{N}{\varepsilon_X \times t \times p_\gamma} \tag{5}$$

where a_X can be either the volumetric activity a_V (Bq m^{-3}) or the superficial activity a_S (Bq m^{-2}), N is the number of counts under the peak, t the counting time, p_γ is the emission probability of the gamma-ray and ε_X is either the volumetric efficiency ε_V or the superficial efficiency ε_S.

Thus, from Eq. (5):

$$\mathrm{MDAC} = \frac{L_D}{\varepsilon_X \times t \times p_\gamma} \tag{6}$$

If the measured spectrum is assumed to be only background, the detection limit L_D (with a 95% confidence limit) for a certain Region of Interest (ROI) in the spectrum can be calculated using the following single-count Currie expression (Currie, 1968):

$$L_D = 2.71 + 4.65\sqrt{B} \tag{7}$$

where B is the number of counts produced by the background in the considered ROI.

The width of the ROI is determined using the width of the expected peak, which is proportional to the $FWHM(E)$ function (obtained from the resolution calibration) of each detector:

$$n = n(E) = k \times FWHM(E) \tag{8}$$

where k is the proportionality constant to set the desired peak coverage and $FWHM(E)$ is obtained in the resolution calibration. For example, $k=2.548$ for a 99.73% peak area coverage.

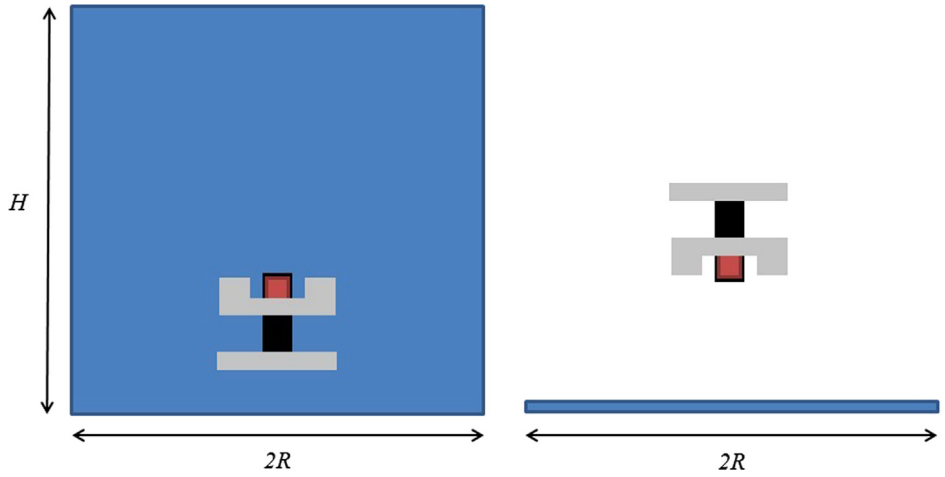

Fig. 3. Geometry of the source term used in the MC simulations for the up-detectors (left) and for the down-detectors (right).

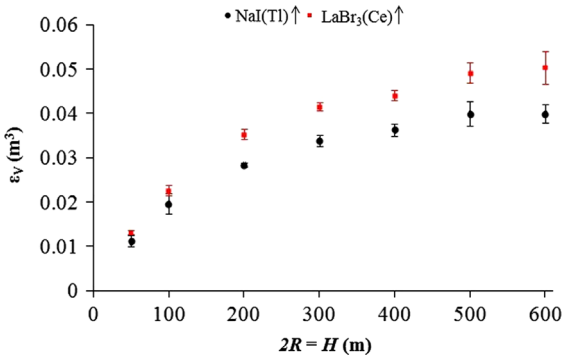

Fig. 4. Variation of the efficiency values with the source term size (homogeneous cylinder of radius R and height H) for a monoenergetic source of 662 keV gamma-rays for the up-detectors.

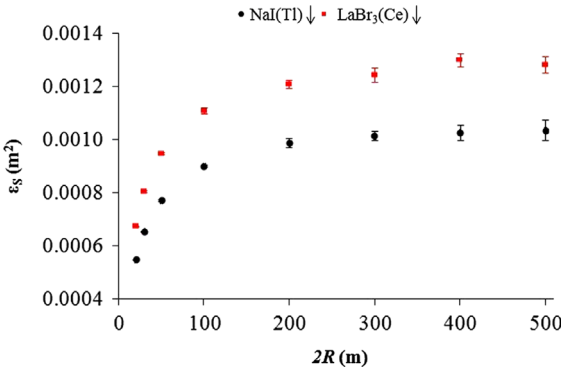

Fig. 5. Variation of the efficiency values with the source term size (homogeneous disk of radius R) for a monoenergetic source of 662 keV gamma-rays for the down-detectors.

3. Results and discussion

3.1. Source term size

The variation of the efficiency values with the source term size for a monoenergetic homogeneous source of 662 keV gamma-rays is shown in Fig. 4 for the up-detectors and in Fig. 5 for the down-detectors.

The obtained results show, in both cases, that the efficiencies increased with the size of the source term. In particular, the observed dependences of the efficiencies with the radius R of the source term were approximately $\varepsilon_V \propto R^{0.5}$ and $\varepsilon_S \propto R^{0.2}$; thus, the variation on the efficiency values reduces as the size of the source term increases.

This can be explained considering that the half-value layer in air for 662 keV gamma-rays is 74 m, which is related to the percentage of photons contributing to efficiency. For example, for distances larger than 250 m, less than 10% of the photons will reach the detector.

Based on these results, the final efficiency curves for the RARM-D2 (see Section 3.2) were calculated using $2R = 500$ m for both NaI (Tl) and $LaBr_3$(Ce) detectors in both configurations (pointing up or down).

3.2. Efficiency calculations

The efficiency curves for the RARM-D2 calculated from the MC simulations are shown in Fig. 6 (up-detectors) and Fig. 7 (down-detectors). The data were well fitted to Eq. (4) (dotted lines in the plots). The coefficients of determining r^2 for the NaI(Tl) fits were 0.997 (up) and 0.9994 (down); these coefficients for the $LaBr_3$(Ce) were 0.997 (up) and 0.9994 (down).

The computation times ranged from 45 min (for 20 keV photons) to 35 h (3000 keV photons) in the NaI(Tl) detectors and from 1.4 h (for 20 keV photons) to 45.4 h (3000 keV photons) in the $LaBr_3$(Ce) detectors.

The calculated efficiencies for the NaI(Tl) were systematically lower than the $LaBr_3$(Ce) efficiencies as a consequence of their different densities, which were 3.67 g cm^{-3} and 5.08 g cm^{-3}, respectively. Below 300 keV, the differences between the NaI(Tl) and $LaBr_3$(Ce) efficiencies were shorter primarily because the attenuation of the gamma-rays in the air and in the detector covers is higher at lower energies.

3.3. Typical spectra

The variability of the background spectra may strongly depend on the meteorological conditions. However (and by way of example), 24 h typical spectra obtained with the RARM-D2 are shown in Fig. 8 for the up-detectors and in Fig. 9 for the down-detectors. Similar count rates were obtained for 10 min spectra, but the quality of the peaks was lower due to low statistics.

The more important observed peaks were from ^{222}Rn and ^{232}Th daughters (such as ^{214}Pb, ^{214}Bi and ^{208}Tl) and from the NORM ^{40}K, especially on the down detectors. In addition, $LaBr_3$(Ce) spectra showed clear evidence of its intrinsic activity, which has been discussed elsewhere (Quarati et al., 2012).

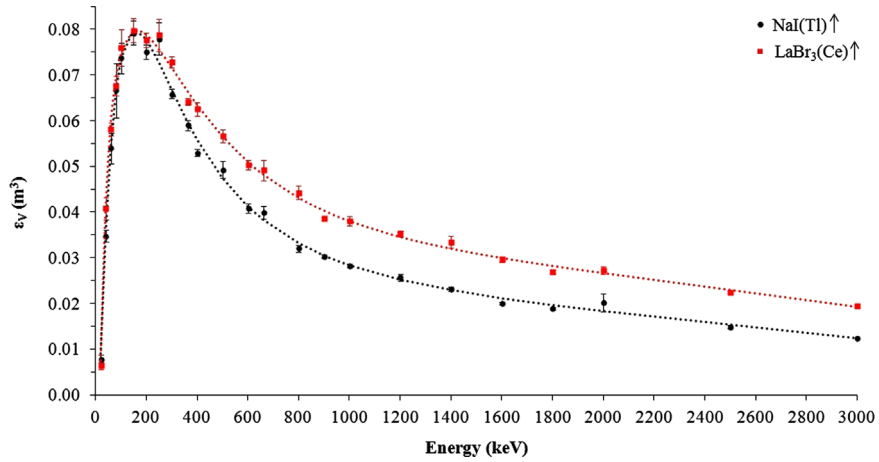

Fig. 6. Efficiency curves calculated using the MC simulations for up NaI(Tl) (black dots) and $LaBr_3(Ce)$ (red squares). The dotted lines correspond to the fit described by Eq. (4). (For interpretation of the references to color in this figure legend, the reader is referred to the web version of this article.)

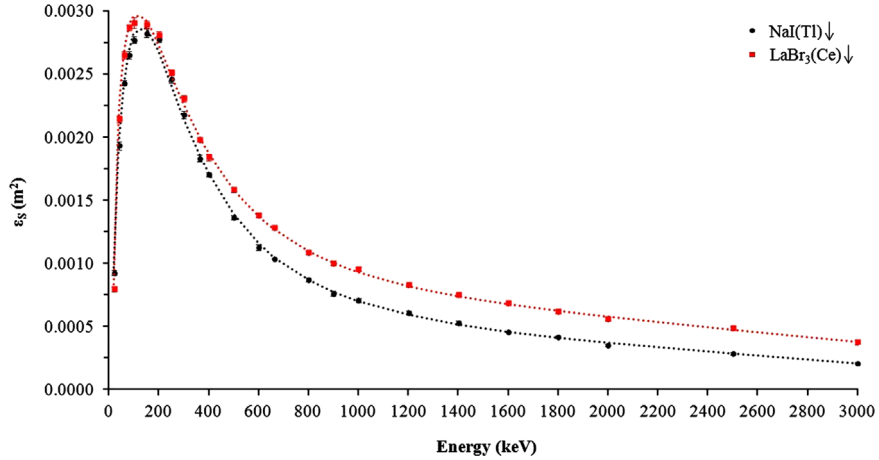

Fig. 7. Efficiency curves calculated using the MC simulations for down NaI(Tl) (black dots) and $LaBr_3(Ce)$ (red squares). The dotted lines correspond to the fit described by Eq. (4). (For interpretation of the references to color in this figure legend, the reader is referred to the web version of this article.)

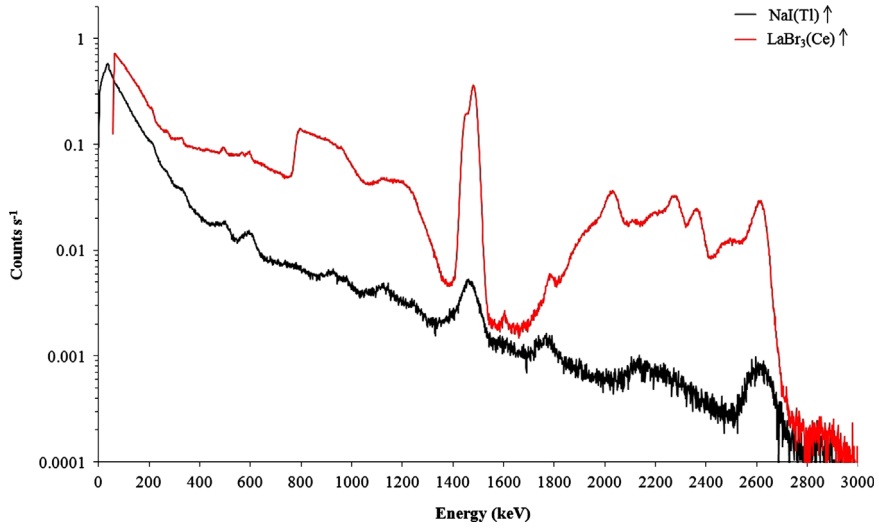

Fig. 8. Spectra of the typical background radiation measured with the pointing-up detectors, NaI(Tl) and $LaBr_3(Ce)$, of the RARM-D2 with an integration time of 24 h.

Better energy resolution was observed in the obtained spectra for the $LaBr_3(Ce)$ detectors than the NaI(Tl) detectors. For example, the $LaBr_3(Ce)$ could resolve the peaks from ^{208}Tl at 583 keV and ^{214}Bi at 609 keV, while the NaI(Tl) detectors could not resolve these peaks.

3.4. MDAC

The measurement capabilities of the RARM-D2 in terms of the MDAC are shown in Table 1 (up-detectors) and in Table 2 (down-detectors) for the ^{131}I and ^{137}Cs isotopes. MDACs were calculated

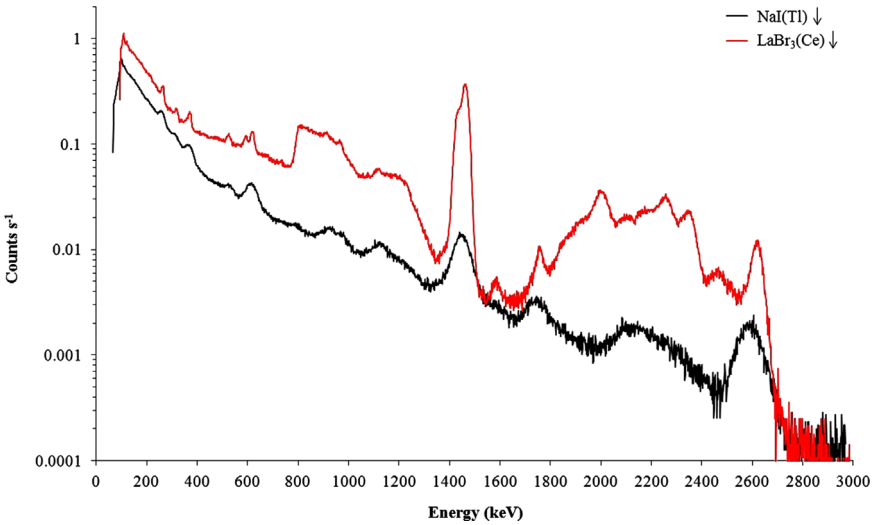

Fig. 9. Spectra of the typical background radiation measured with the pointing-down detectors, NaI(Tl) and $LaBr_3$(Ce), of the RARM-D2 with an integration time of 24 h.

Table 1
MDAC values for the ^{131}I and ^{137}Cs isotopes in the up-detectors at different integration times.

Integration time	MDAC (Bq m^{-3})			
	NaI(Tl)		$LaBr_3$(Ce)	
	^{131}I (365 keV)	^{137}Cs (662 keV)	^{131}I (365 keV)	^{137}Cs (662 keV)
10 min	4.89 ± 0.09	5.3 ± 0.2	5.25 ± 0.07	6.5 ± 0.3
1 h	1.97 ± 0.04	2.14 ± 0.07	2.12 ± 0.03	2.63 ± 0.12
4 h	0.98 ± 0.02	1.06 ± 0.04	1.05 ± 0.01	1.31 ± 0.06
12 h	0.57 ± 0.01	0.61 ± 0.02	0.61 ± 0.01	0.76 ± 0.03
24 h	0.40 ± 0.01	0.43 ± 0.01	0.43 ± 0.01	0.53 ± 0.02

Table 2
MDAC values for the ^{131}I and ^{137}Cs isotopes in the down-detectors at different integration times.

Integration time	MDAC (Bq m^{-2})			
	NaI(Tl)		$LaBr_3$(Ce)	
	^{131}I (365 keV)	^{137}Cs (662 keV)	^{131}I (365 keV)	^{137}Cs (662 keV)
10 min	288 ± 4	342 ± 6	238 ± 2	278 ± 3
1 h	117 ± 2	138 ± 3	96.6 ± 0.9	112 ± 1
4 h	58.3 ± 0.8	69 ± 1	48.2 ± 0.5	56.0 ± 0.7
12 h	33.6 ± 0.5	39.8 ± 0.7	27.8 ± 0.3	32.3 ± 0.4
24 h	23.8 ± 0.2	28.1 ± 0.5	19.6 ± 0.2	22.8 ± 0.3

using Eqs. (6)–(8) over typical spectra obtained at different integration times. The spectra were assumed to be only background, and a value of $k = 2.548$ (99.73% of the peak area coverage) was used. This value was chosen to ensure a full coverage of the hypothetical peak (smaller values could underestimate the background under it).

The most significant contribution to the MDACs uncertainty is the efficiency value component, which could be reduced using a larger number of histories in the simulations.

When comparing the MDACs for the up-detectors, the MDAC values were systematically higher for the $LaBr_3$(Ce) detector than for the NaI(Tl) detector. This is a consequence of the intrinsic activity of the former, which produces an additional background to the spectra that raises the number of counts in the studied ROIs. In contrast, the MDAC values in the down-detectors were systematically lower for the $LaBr_3$(Ce) detector than for the NaI(Tl) detector; the natural background in the down-detectors is higher than in the up-detectors. Thus, the natural component of the background predominates in front of the intrinsic background of the $LaBr_3$(Ce) in the considered ROIs and is equivalent for both detectors; hence, the better resolution and the larger efficiency of the $LaBr_3$(Ce) improve the MDACs.

4. Conclusions

A Real-time Airborne Radioactivity Monitor using Direct gamma-ray spectrometry with two scintillation detectors (RARM-D2) was developed. The RARM-D2 is formed using two scintillation detectors, either NaI(Tl) or $LaBr_3$(Ce), with one pointing up and the other pointing down, which are shielded with Pb. This disposition permits the discrimination between the isotopes contained in a radioactive cloud from those deposited or emerging from the ground.

The RARM-D2 was fully calibrated using experimental data except for the efficiency curve, which was set using Monte Carlo simulations with the EGS5 code system that reproduced the responses of the NaI(Tl) and $LaBr_3$(Ce) detectors. Prior to setting the efficiency curve, the effect of the radioactive source term size on the efficiency calculations was studied for the gamma-rays from ^{137}Cs, either for the up-detectors or for the down detectors. This approach made it possible to set a reasonable infinite homogeneous source, which was used to set the entire efficiency curve up to 3000 keV for all studied detectors.

Using the calculated efficiency curves, the capabilities of the RARM-D2 were evaluated with some MDAC calculations over average spectra and for different integration times. This evaluation was performed for all configurations (up and down) of NaI(Tl) and $LaBr_3$(Ce) measuring ^{131}I and ^{137}Cs.

Finally, the RARM-D2 is ready to be used in an automatic real-time environmental radiation surveillance network. The design of the RARM-D2 enables a primary characterization of the radioactive source term and permits a comparison of the obtained data with the legal limits established for the activity concentrations, thereby allowing alarm levels for early warning to be established.

Acknowledgements

Some of this research was performed using the resources of CESCA (Centre de Supercomputació de Catalunya).

References

2000/473/Euratom, 27 July 2000. Commission Recommendation of 8 June 2000, Official Journal of the European Commission, No. 191. Available from: ⟨http://ec.europa.eu/energy/nuclear/radioprotection/doc/legislation/00473_en.pdf⟩.

Aage, H.K., Korsbech, U., Bargholz, K., 2003. Early detection of radioactive fallout by gamma spectrometry. Radiat. Prot. Dosim. 106, 155–164.

Berger, M.J., Coursey, J.S., Zucker, M.A., Chang, J., 2005. ESTAR, PSTAR, and ASTAR: Computer Programs for Calculating Stopping-Power and Range Tables for Electrons, Protons, and Helium Ions (version 1.2.3). National Institute of Standards and Technology, Gaithersburg, Available from: ⟨http://physics.nist.gov/Star⟩

Casanovas, R., Morant, J.J., Lopez, M., Hernandez-Giron, I., Batalla, E., Salvadó, M., 2011. Performance of data acceptance criteria over 50 months from an automatic real-time environmental radiation surveillance network. J. Environ. Radioact. 102, 742–748.

Casanovas, R., Morant, J.J., Salvadó, M., 2012a. Energy and resolution calibration of NaI(Tl) and $LaBr_3$(Ce) scintillators and validation of an EGS5 Monte Carlo user code for efficiency calculations. Nucl. Instrum. Methods Phys. Res., Sect. A 675, 78–83.

Casanovas, R., Salvadó, M., Lopez, M. Estación de identificación y medida en tiempo real de la radiactividad ambiental gamma, mediante espectrometría con dos cristales de centelleo (in Spanish). ES Patent Application P201230236, 15th February 2012b. Available from: ⟨http://www.oepm.es/pdf/ES/0000/000/02/42/32/ES-2423236_A1.pdf⟩.

Casanovas, R., Salvadó, M., Lopez, M., Tapia, C., de Blas, A. Estación de identificación y medida en tiempo real de la radiactividad ambiental gamma mediante espectrometría sobre filtro de papel (in Spanish). ES Patent Application P201230408, 16th March 2012c. Available from: ⟨http://www.oepm.es/pdf/ES/0000/000/02/42/58/ES-2425801_A1.pdf⟩.

Casanovas, R., Morant, J.J., Salvadó, M., 2012d. Temperature peak-shift correction methods for NaI(Tl) and $LaBr_3$(Ce) gamma-ray spectrum stabilisation. Radiat. Meas. 47, 588–595.

Casanovas, R., Morant, J.J., Salvadó, M. Development and calibration of a real-time airborne radioactivity monitor using gamma-ray spectrometry on a particulate filter. IEEE Transactions on Nuclear Science (2014). http://dx.doi.org/10.1109/TNS.2014.2299715.

Casanovas, R., Morant, J.J., Salvadó, M., 2013. Implementation of gamma-ray spectrometry in two real-time water monitors using NaI(Tl) scintillation detectors. Appl. Radiat. Isot. 80, 49–55.

Currie, L.A., 1968. Limits for qualitative detection and quantitative determination. Anal. Chem. 40, 586–593.

Mattila, A., Toivonen, H., Vesterbacka, K., Leppänen, M., Salmelin, S., Pelikan, A. Radiation monitoring network with spectrometric capabilities: implementation of $LaBr_3$ spectrometers to the Finnish network. In: Proceedings of the Third European IRPA Congress, 2010, Helsinki, Finland. Available from: ⟨http://www.irpa2010europe.com/pdfs/proceedings/S12-P12.pdf⟩.

Quarati, F.G.A., Khodyuk, I.V., van Eijk, C.W.E., Quarati, P., Dorenbos, P., 2012. Study of ^{138}La radioactive decays using $LaBr_3$ scintillators. Nucl. Instrum. Methods Phys. Res., Sect. A 683, 46–52.

Toivonen, H., Vesterbacka, K., Pelikan, A., Mattila, A., Karhunen, T. $LaBr_3$ spectrometry for environmental monitoring. In: Proceedings of the 12th International Congress of the International Radiation Protection Association, 2008, Buenos Aires, Argentina. Available from: ⟨http://www.irpa12.org.ar/fullpapers/FP0611.pdf⟩.

Zhang, W., Korpach, E., Berg, R., Ungar, K., 2013. Testing of an automatic outdoor gamma ambient dose-rate surveillance system in Tokyo and its calibration using measured deposition after the Fukushima nuclear accident. J. Environ. Radioact. 125, 93–98.